

Research



Cite this article: Novak I, Truskinovsky L. 2017 Segmentation in cohesive systems constrained by elastic environments. *Phil. Trans. R. Soc. A* **375**: 20160160.
<http://dx.doi.org/10.1098/rsta.2016.0160>

Accepted: 6 December 2016

One contribution of 13 to a theme issue 'Patterning through instabilities in complex media: theory and applications'.

Subject Areas:

mechanics

Keywords:

fracture, competing interactions, segmentation, elastic foundation

Author for correspondence:

L. Truskinovsky
e-mail: lev.truskinovsky@espci.fr

Segmentation in cohesive systems constrained by elastic environments

I. Novak¹ and L. Truskinovsky²

¹Department of Cell Biology, University of Connecticut, Farmington, CT 06030, USA

²Physique et Mécanique des Milieux Hétérogènes, CNRS-UMR 7636, PSL, ESPCI, 10 Rue Vauquelin, 75005 Paris, France

 LT, 0000-0003-0852-176X

The complexity of fracture-induced segmentation in elastically constrained cohesive (fragile) systems originates from the presence of competing interactions. The role of discreteness in such phenomena is of interest in a variety of fields, from hierarchical self-assembly to developmental morphogenesis. In this paper, we study the analytically solvable example of segmentation in a breakable mass–spring chain elastically linked to a deformable lattice structure. We explicitly construct the complete set of local minima of the energy in this prototypical problem and identify among them the states corresponding to the global energy minima. We show that, even in the continuum limit, the dependence of the segmentation topology on the stretching/pre-stress parameter in this problem takes the form of a devil's type staircase. The peculiar nature of this staircase, characterized by locking in rational microstructures, is of particular importance for biological applications, where its structure may serve as an explanation of the robustness of stress-driven segmentation.

This article is part of the themed issue 'Patterning through instabilities in complex media: theory and applications'.

1. Introduction

In materials science, considerable efforts have been focused on the study of pattern formation induced by fracturing in brittle structures reinforced by elastic elements/environments. Under quasi-static loading, such composite systems show a peculiar response: while one phase carries the load, another one fractures

sequentially with emerging discontinuities forming a regular segmentation pattern. Typical examples include cracking of drying mud, fragmentation of thin coatings and rupture of fibres in elastic matrices [1–3].

Recently, it was realized that conceptually similar phenomena take place during drying-induced hierarchical self-assembly in nano-bristle assemblages, from carbon nanotube forests to gecko feet hairs. These discrete systems were shown to exhibit remarkable robustness of sequential assembly with the characteristic locking on particular patterns, which could be reached and maintained reliably [4–6].

An even more recent domain of application for fracture-induced patterning is developmental morphogenesis, where differential growth appears to be at least partially responsible for such segmentation phenomena as leaf venation and formation of vertebra. Here the locking phenomena, ensuring robust reproducibility of the developmental patterns, are again of crucial importance [7–9]. The biological applications of this mechanism of segmentation go beyond growth phenomena; for instance, non-trivial mechanics may also be involved in self-organization of the sarcomeres in skeletal muscles operating on the descending limb [10].

The established models of decohesion-induced patterning in partially brittle systems rely predominantly on a continuum mechanical description. The effects of discreteness have so far been addressed almost exclusively in the context of inhomogeneity of fracture thresholds with the focus on the dependence of the statistical structure of the emerging patterns on the properties of quenched disorder. In these studies, the description of the non-brittle part of the system is usually oversimplified (rigid foundation), and fracture is perceived as a set of irreversible transitions involving marginal metastable states [11–13]. The existing analytical results mostly concern linear stability, while stable patterning has been studied mostly numerically; for a successful realization of this programme, see, for instance, [14].

The goal of this paper is to understand the universal features of the complex energy landscapes in such systems, with the focus on discreteness rather than on quenched disorder. In an attempt to elucidate the origin of the locking phenomena, we consider, in this paper, a prototypical one-dimensional scalar model amenable to a fully analytical study. Taken literally, the model describes a chain of breakable springs linked elastically to an unbreakable elastic foundation, which is modelled as another chain with unbreakable springs [15]. The naive continuum analogue of this system would be a long thin strip of rubber (representing the unbreakable layer) with a strip of glass (representing the breakable layer) glued on top of it. Upon stretching of this bilayer sandwich structure from the two ends, the glass is expected to break into pieces of roughly uniform length, and the discrete model can be viewed as a simple mathematical description for this phenomenon. However, our study of the continuum limit reveals the effects that cannot be captured by the apparently straightforward analogy with the classical continuum fracture mechanics.

The model is sufficiently transparent mathematically to reveal the inherent complexity of the energy landscape, which turns out to be rugged even in the absence of quenched disorder. In particular, we could identify the complete set of metastable states (local minima of the energy) and specify among them the ground states (global energy minima). Our main interest is in the dependence of the energy-minimizing patterns on the stretching/pre-stress parameter. We show that in the continuum limit it exhibits some features of an incomplete devil's staircase. While this rather remarkable trace of the underlying discreteness is beyond reach of the naive quasi-continuum approaches, the ensuing locking in rational microstructures is of great importance for biological applications, where it may serve as an explanation for the robustness of particular patterns during stress-driven segmentation.

Our study of the toy model reveals a qualitative relation between the phenomenon of parametric locking and the presence in the system of environment-induced interactions of antiferromagnetic type. However, the specific quantitative predictions of the model should be interpreted with caution because of its schematic nature; for instance, the stress decay in the scalar one-dimensional case is exponential instead of the conventional power law, and new fracture

cannot take place near an existing one as is the case in three-dimensional models [16]. More detailed modelling is needed to either affirm or renounce our simplifying assumptions.

The paper is organized as follows. In §2, we formulate the model and map it on a zero-temperature Ising model with long-range interactions. After minimizing out linear variables, we compute in §3 the complete set of metastable states for the general finite-size system. Segmentation patterns potentially contributing to the global minimization of the energy are identified in §4. The ultimate selection of the ground states is performed in §5. The concluding section contains the summary of the results.

The analysis of a similar discrete system where the ‘breakable springs’ are replaced by ‘bistable springs’ is conducted in a companion paper [9].

2. The model

In a strictly minimal framework, we can model the cohesive/brittle component of the composite system by a simple one-dimensional mass–spring chain with breakable springs. To represent in the same setting the load-carrying background, we assume that the nodes of the chain (masses) are connected by leaf springs to a parallel linear elastic (unbreakable) chain (figure 1). Both chains are loaded symmetrically in the common hard device, which applies displacements to the boundary nodes; the value of the macroscopic strain then serves as the loading parameter. An equivalent formulation can be obtained if the system is placed in a fixed device and loaded internally through the pre-strain as in the case of differential growth or drying.

As the macroscopic strain increases, the cohesive/brittle layer is expected to break into fragments whose number depends on the value of the load. The assumption that the system is in metastable equilibrium at each value of the loading parameter does not fix the number of fragments because of the ruggedness of the underlying energy landscape. To fix the configuration at a given load, we need to specify the dynamics of the system and account for its previous history. Our particular focus will be on the evolution, presuming that independently of the value of the loading parameter the system remains in the ground state (the state of the global minimum of the energy). This ‘equilibrium’ strategy, which excludes history dependence, can be viewed as a limit of the finite-temperature Hamiltonian (stochastic) dynamics as both the environmental temperature and the rate of loading tend to zero.

In dimensionless form, the energy density of the system can be written as

$$\bar{w}(\mathbf{u}, \mathbf{v}, N) = N^{-1} \sum_{i=1}^N \left[w(u_i - u_{i-1}) + \frac{1}{2} E_{\perp} (u_i - v_i)^2 + \frac{1}{2} E_{\parallel} (v_i - v_{i-1})^2 \right], \quad (2.1)$$

where u_i is the displacement of the i th node of the brittle chain, v_i is the displacement of the i th node of the unbreakable elastic background and N is the number of elements in each of the chains. Often, energies like (2.1) are written in the rescaled variables $N^{-1}u_i$ and $N^{-1}v_i$ (see for instance a study of the brittle chain without the background in [17]), but here we do not find this additional rescaling necessary.

In equation (2.1), we denoted by w the energy of the Lennard-Jones type, by E_{\perp} the (shear) elastic modulus of a leaf spring connecting two chains and by E_{\parallel} the Young modulus of the parallel linear elastic springs. The reference lengths of all the linear elements are assumed to be the same, and this parameter is used as a length scale in the non-dimensionalization of the problem. When $E_{\perp} \rightarrow \infty$ and $u_i \rightarrow v_i$, we obtain a single chain with double-well springs [18]. If instead $E_{\parallel} \rightarrow \infty$ and $v_i \rightarrow v_{i-1}$, we obtain a Frenkel–Kontorova-type problem with a quadratic on-site potential and a non-convex interparticle potential [19]. For general finite E_{\perp} and E_{\parallel} , the linear variables v_i can be minimized out, leading to a model with a single set of variables u_i subjected to long-range antiferromagnetic interactions.

The simplest model of a breakable spring is a ‘fuse’ that deforms linearly till the critical value of the force/elongation. Here we consider a slightly more realistic trilinear spring model with the

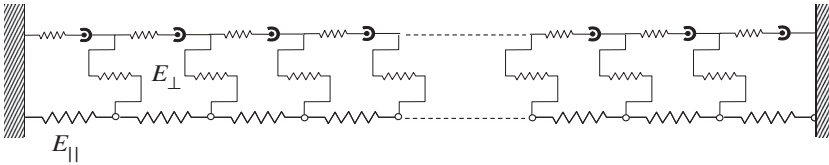


Figure 1. Schematic of a breakable structure elastically linked to a deformable background.

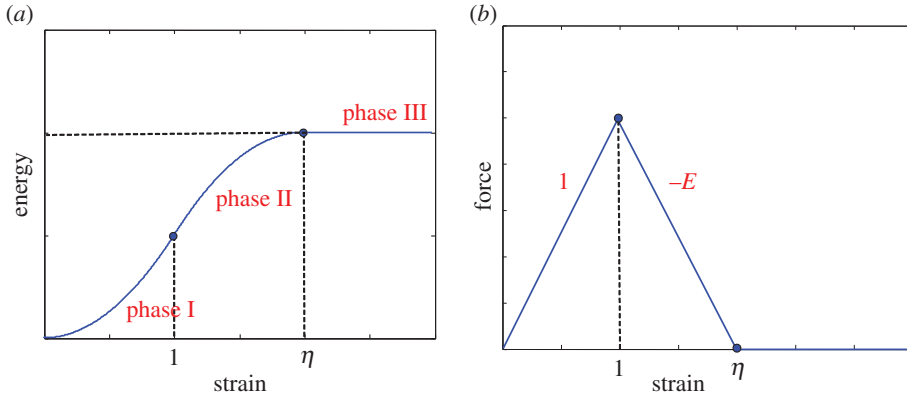


Figure 2. (a) The energy–strain and (b) the force–strain relations for an individual cohesive/brittle spring. (Online version in colour.)

energy

$$w(x) = \begin{cases} \frac{1}{2}x^2, & x \leq 1, \\ -\frac{(x-\eta)^2}{2(\eta-1)} + \frac{\eta}{2}, & 1 < x < \eta, \\ \frac{\eta}{2}, & x \geq \eta, \end{cases} \quad (2.2)$$

which becomes the energy of a fuse in the special case $\eta = 1$. For $\eta > 1$, the energy (2.2) is illustrated in figure 2, where we identified three ‘phases’, intact (phase I), spinodal (phase II) and broken (phase III), with the respective dimensionless elastic moduli equal to 1 (the corresponding modulus is used as a scale), $-1/(\eta - 1)$ and 0.

Suppose now that on both ends $i = 1$ and $i = N$ the ‘ \mathbf{u} ’- and ‘ \mathbf{v} ’-chains are rigidly connected, and that the whole system is loaded in a hard device so that

$$u_0 = v_0 = 0, \quad u_N = v_N = N\bar{\varepsilon}.$$

The controlling parameter is then the total strain $\bar{\varepsilon}$ and the static problem of elasticity theory reduces to finding

$$\bar{w}(\bar{\varepsilon}, N) = \min_{\substack{\{u_i, v_i, u_0 = v_0 = 0, \\ u_N = v_N = N\bar{\varepsilon}\}}} \bar{w}(\mathbf{u}, \mathbf{v}, N). \quad (2.3)$$

Here the minimization will be first understood in the sense of local minima (metastable states). To this end, we need to solve the system of equilibrium equations

$$\frac{\partial \bar{w}}{\partial u_i} = \frac{\partial \bar{w}}{\partial v_i} = 0,$$

which can be rewritten as

$$\left. \begin{aligned} w'(u_i - u_{i-1}) - w'(u_{i+1} - u_i) + E_{\perp}(u_i - v_i) &= 0 \\ E_{\parallel}(2v_i - v_{i+1} - v_{i-1}) + E_{\perp}(v_i - u_i) &= 0. \end{aligned} \right\} \quad (2.4)$$

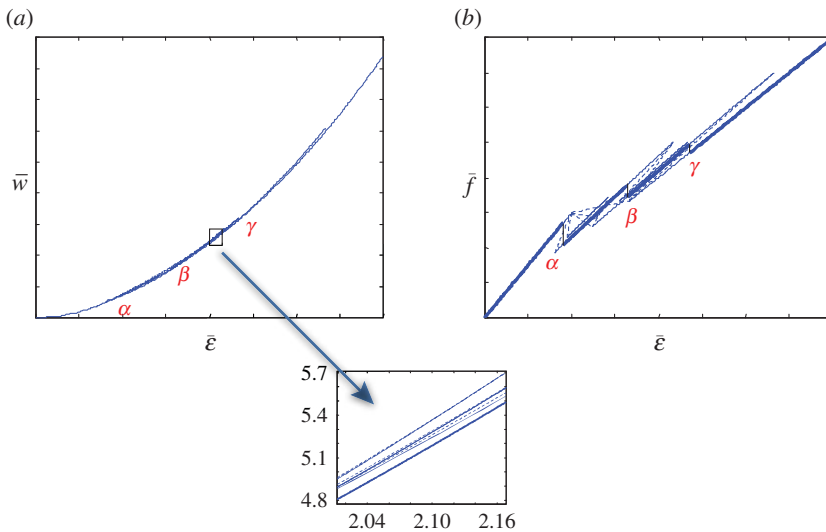


Figure 3. Overall elastic energy–strain relation $\bar{w}(\bar{\epsilon})$ and the force–strain relation $\bar{f}(\bar{\epsilon})$ for the case $N=3$, with $E=1.5$, $E_{\parallel}=2$, $E_{\perp}=1$. Inset below shows the enlarged rectangle in (a). Metastable states are shown with solid lines, unstable states with dashed lines, and absolute minima with bold lines. (Online version in colour.)

A representative solution of equations (2.4) for $N=3$ is illustrated in figure 3a, where we show the energy of all equilibrium states $\bar{w}(\bar{\epsilon})$.

In figure 3b, we show the derivative of this energy $\bar{f}(\bar{\epsilon})$ defining the total force exerted on the loading device. One can see that the equilibrium configurations, containing all three phases I, II and III, may be rather numerous for some values of the loading parameter. To illustrate better the associated difference in the energy levels, it is convenient to subtract from the total energy the homogeneous component mimicking the response of the linear elastic foundation. The remaining ‘apparent energy’ of the brittle layer is then

$$\bar{w}_a(\bar{\epsilon}) = \bar{w}(\bar{\epsilon}) - \frac{1}{2}E_{\parallel}\bar{\epsilon}^2. \quad (2.5)$$

Its derivative,

$$\bar{f}_a(\bar{\epsilon}) = \bar{f}(\bar{\epsilon}) - E_{\parallel}\bar{\epsilon}, \quad (2.6)$$

gives the ‘apparent stress’ exerted by the brittle layer on the loading device. Both functions are illustrated in figure 4a,b for the case $N=3$. In figure 4c, we reproduce figure 4b without unstable configurations, the latter can be easily identified by checking the positive definiteness of the associated Hessian matrix.

The numerical solution of equations (2.4), illustrated in figure 4a–c, reveals the degree of non-uniqueness of the metastable states at a given value of the loading parameter $\bar{\epsilon}$ and shows that the overlapping metastable equilibria form isolated branches (e.g. BC, DE, etc.). In this situation, even if the loading parameter is varied quasi-statically, a branch-switching strategy is needed to fix the evolution of the system. In particular, the (athermal) overdamped strategy, assuming that a metastable branch is followed till it becomes unstable (at points A–E, etc.), is different from the global energy minimization strategy shown in figure 4 by the bold lines ($\alpha\beta$, $\beta\gamma$, etc.).

Because the number of solutions of the nonlinear system (2.4) increases exponentially with N , the visualization of the whole set of equilibrium configurations soon becomes problematic. Among those, configurations containing phases I and III are relevant, because one can show that all of them correspond to local minima of the energy. One can also show that configurations containing a single element in the spinodal region (phase II) can be stable only if the force–strain curve in the spinodal region is sufficiently shallow. In this paper, we do not present the exact conditions on the elastic moduli ensuring that phase II is irrelevant for metastability at a given N ,

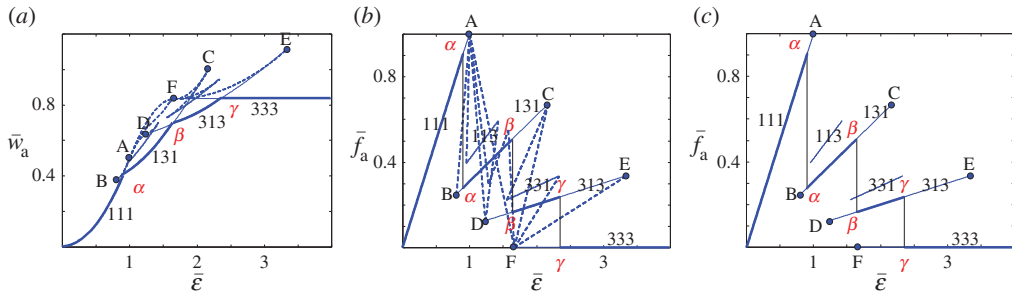


Figure 4. (a) The apparent energy–strain relation $\bar{w}_a(\bar{\varepsilon}) = \bar{w}(\bar{\varepsilon}) - \frac{1}{2}E_{\parallel}\bar{\varepsilon}^2$ and (b) the apparent force–strain relation $\bar{f}_a(\bar{\varepsilon}) = \bar{f}(\bar{\varepsilon}) - E_{\parallel}\bar{\varepsilon}$ for the case $N = 3$; other parameters are $E = 1.5, E_{\parallel} = 2, E_{\perp} = 1$. Metastable states are shown with solid lines, unstable states with dashed lines, and absolute minima with bold lines. Triples of numbers next to solid lines represent the ‘phase’ structure of the configuration: the number 1 stands for phase I and the number 3 for phase III. (c) The apparent force–strain relation with only metastable branches (local energy minima) shown (see a similar graph for $N = 9$ in figure 8b). (Online version in colour.)

which in view of our goals have only technical interest. Instead, in order to maximally simplify the problem and to be able to map the mechanical system onto a spin system, we make an assumption that elastically our cohesive/brittle elements are so close to fuses that we can ignore the possibility that there are metastable states involving phase II.

3. Metastable states

Because we now deal with phases I and III only, it is natural to introduce a spin variable S such that

$$S = \begin{cases} -1, & \text{for phase I,} \\ 1, & \text{for phase III.} \end{cases}$$

In this way, we can parametrize all metastable microconfigurations by a succession of integers 1 and -1 . Given $\mathbf{S} = \|S_1, S_2, \dots, S_N\|$ we can explicitly solve the linear system (2.4) and reformulate the problem as the Ising model with non-local interactions.

Springs in phase III generate zero force and divide the brittle subsystem into segments (phase I ‘islands’ that may contain only one point) that do not interact and can be permuted (figure 5). To describe a microconfiguration of such a partially broken chain, it is sufficient to specify a set of integers n_i representing the numbers of phase I springs between two successive phase III springs. We also suppose that the two integers n_0 and n_m prescribe the sizes of the phase I ‘islands’ at the ends of the chain. When two elements in phase III are adjacent to each other, we would say that the corresponding n_i is equal to zero. The total number of the phase I islands will then be $m + 1$, where the parameter

$$m = \sum_{i=1}^N \frac{S_i + 1}{2},$$

represents the total number of broken elements (analogue of magnetization). It can be found from the condition

$$\sum_{i=0}^m n_i + m(\mathbf{n}) = N.$$

Suppose now that the geometrical configuration of the system is specified, i.e. the values of all $n_i, i = 0, \dots, m$, are given. The solution of the linear problem inside each ‘island’ (shown in more detail in figure 6) reduces to the inversion of a tridiagonal matrix and it can be written explicitly.

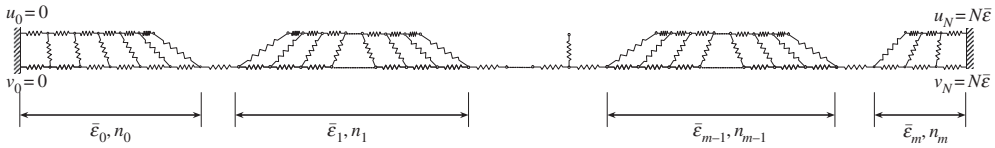


Figure 5. Partially broken system containing cohesive/brittle springs in phases I and III only.

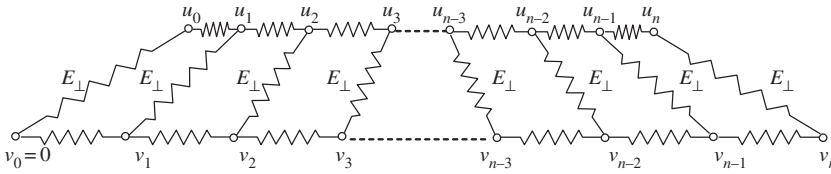


Figure 6. Interior 'island' containing cohesive/brittle springs in phase I only. Dashed lines indicated the omitted interior points of the island.

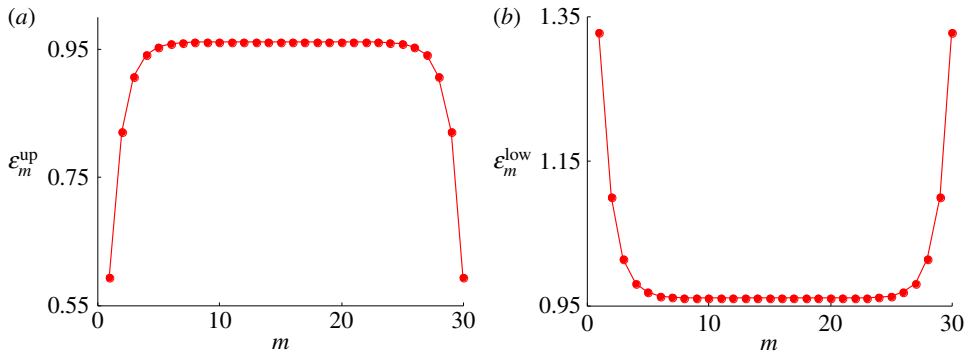


Figure 7. Typical strain distributions inside an interior 'island' containing only phase I springs: (a) brittle (upper) layer, (b) elastic background (lower layer). (Online version in colour.)

For the interior islands, after straightforward computations (similar to the ones presented in [20]), we obtain

$$u_j = j\bar{\epsilon}_i - \bar{\epsilon}_i \frac{(2j - n_i) \sinh n_i \theta + E_{\parallel} n_i \sinh(2j - n_i) \theta}{2 \sinh n_i \theta + 2E_{\parallel} n_i \sinh \theta \cosh(n_i + 1) \theta}$$

$$\text{and } v_j = j\bar{\epsilon}_i - \bar{\epsilon}_i \frac{(2j - n_i) \sinh n_i \theta - n_i \sinh(2j - n_i) \theta}{2 \sinh n_i \theta + 2E_{\parallel} n_i \sinh \theta \cosh(n_i + 1) \theta},$$

where $\bar{\epsilon}_i$ is the average strain inside the i th 'island'. Here, we have introduced the parameter

$$\theta = \sinh^{-1} \left(0.5 \sqrt{\frac{E_{\perp}(1 + E_{\parallel})}{E_{\parallel}}} \right),$$

which defines the normalized internal length. It characterizes, for instance, the size of the boundary layers illustrated in figure 7.

Using Clapeyron's theorem, we can now compute explicitly the energy of an interior (phase I) 'island' as

$$\bar{w}^*(\bar{\epsilon}_i, n_i) = \frac{1}{2} n_i C(n_i) \bar{\epsilon}_i^2, \quad (3.1)$$

where

$$C(n_i) = \frac{n_i E_{\parallel} (E_{\parallel} + 1)}{n_i E_{\parallel} + \tanh[(n_i + 1)\theta] \coth \theta - 1}.$$

For the two boundary ‘islands’, we obtain

$$\bar{w}^{**}(\bar{\varepsilon}_0, n_0) = \bar{w}^*(\bar{\varepsilon}_0, 2n_0), \quad \bar{w}^{**}(\bar{\varepsilon}_m, n_m) = \bar{w}^*(\bar{\varepsilon}_m, 2n_m).$$

We can then express the total energy of the partially equilibrated system in the form

$$\tilde{w}(\{\bar{\varepsilon}_i\}, \varepsilon, \mathbf{n}) = \frac{1}{N} \sum_{i=1}^{m-1} \bar{w}^*(\bar{\varepsilon}_i, n_i) + \frac{1}{2N} \bar{w}^*(\bar{\varepsilon}_0, 2n_0) + \frac{1}{2N} \bar{w}^*(\bar{\varepsilon}_m, 2n_m) + \left(\frac{E_{\parallel}}{2} \varepsilon^2 + \frac{\eta}{2} \right) \frac{m}{N}. \quad (3.2)$$

Here, ε is the strain in the elements of the elastic foundation opposing the regions where the brittle components of the system are broken.

The next step is to find the minimum of (3.2) with respect to the remaining elastic parameters $\bar{\varepsilon}_i$ and ε , which are subjected to the constraint

$$N\bar{\varepsilon} = \sum_{i=0}^m \bar{\varepsilon}_i n_i + \varepsilon m. \quad (3.3)$$

Because the function $\tilde{w}(\{\bar{\varepsilon}_i\}, \varepsilon, \mathbf{n})$ is quadratic with respect to these parameters, its minimization reduces to the solution of the linear system of equations

$$\left. \begin{aligned} \bar{\varepsilon}_0 C(2n_0) &= \bar{f}, \\ \bar{\varepsilon}_i C(n_i) &= \bar{f}, \quad i = 1, \dots, m-1, \\ \bar{\varepsilon}_m C(2n_m) &= \bar{f}, \\ E_{\parallel} \varepsilon &= \bar{f}, \\ \sum_{i=0}^m \bar{\varepsilon}_i n_i + \varepsilon m &= N\bar{\varepsilon}, \end{aligned} \right\} \quad (3.4)$$

where \bar{f} represents the force acting on the loading device. After a lengthy but straightforward computation, we obtain the expression of the relaxed elastic energy in terms of the ‘geometrical parameters’ \mathbf{n} ,

$$\bar{w}(\bar{\varepsilon}, \mathbf{n}) = \frac{E_{\parallel} (1 + E_{\parallel})}{2(E_{\parallel} + \phi(\mathbf{n}, m(\mathbf{n})))} \bar{\varepsilon}^2 + \frac{\eta m(\mathbf{n})}{2N}, \quad (3.5)$$

where

$$\phi(\mathbf{n}, m(\mathbf{n})) = \frac{1}{N \tanh \theta} \left[\sum_{i=1}^{m-1} \tanh(n_i + 1)\theta + \frac{\tanh(2n_0 + 1)\theta + \tanh(2n_m + 1)\theta}{2} \right]. \quad (3.6)$$

The force \bar{f} can also be found explicitly:

$$\bar{f}(\bar{\varepsilon}, \mathbf{n}) = \frac{d\bar{w}(\bar{\varepsilon}, \mathbf{n})}{d\bar{\varepsilon}} = \frac{E_{\parallel} (1 + E_{\parallel})}{E_{\parallel} + \phi(\mathbf{n}, m(\mathbf{n}))} \bar{\varepsilon}. \quad (3.7)$$

As we have already mentioned, each equilibrium configuration parametrized by the integer-valued vector \mathbf{n} corresponds to a local minimum of the energy. Therefore, the linear force–elongation relations given by equation (3.7) describe different metastable branches of equilibria. An example showing the complexity of the complete set of metastable branches is presented in figure 8 for the chain with $N = 9$; to distinguish individual metastable branches, we now show only the apparent elastic energy and the apparent force–strain relation. The two-side limits in $\bar{\varepsilon}$ for the metastable branches (3.7) can be obtained explicitly for general N . They play a crucial role in the case of overdamped quasi-static dynamics, when the system remains in a local minimum till the latter ceases to exist; however, in view of our focus on the global minima of the energy, we can omit this information here.

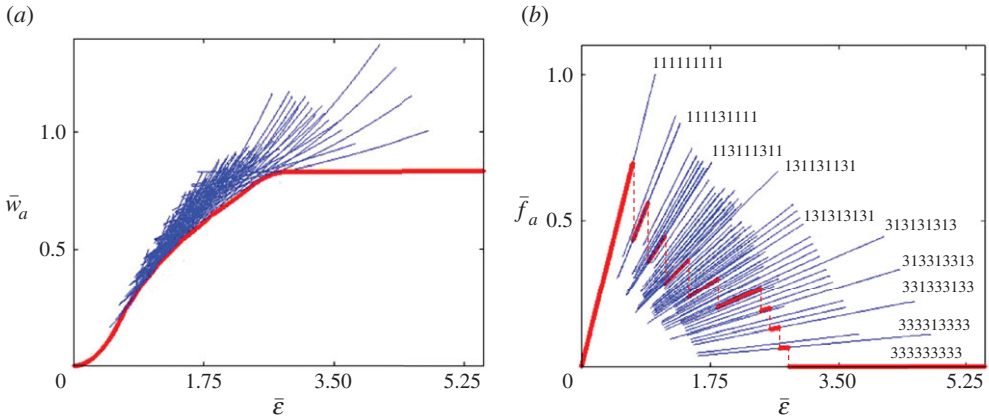


Figure 8. (a) The apparent elastic energy–strain relation $\bar{w}_a(\bar{\epsilon}) = \bar{w}(\bar{\epsilon}) - \frac{1}{2}E_{\parallel}\bar{\epsilon}^2$ and (b) the apparent active force–strain relation $\bar{f}_a(\bar{\epsilon}) = \bar{f}(\bar{\epsilon}) - E_{\parallel}\bar{\epsilon}$ for the metastable branches in the system with $N = 9$. Absolute minima are shown with thick red lines; unstable states, in contrast to figure 3b, are omitted. Sequences of numbers in (b) represent the structure of the global minimizers: the number 1 stands for phase I and the number 3 for phase III (see a similar graph for $N = 3$ in figure 4c). (Online version in colour.)

4. Global minimization

To find the global minimum of the energy at a given $\bar{\epsilon}$, we need to compare the energies of the metastable states $\bar{w}(\bar{\epsilon}, \mathbf{n})$ corresponding to different ‘geometries’ \mathbf{n} . The special structure of (3.5) suggests that we first fix the order parameter m and find

$$\bar{w}(\bar{\epsilon}, m) = \min_{\mathbf{n}} \bar{w}(\bar{\epsilon}, \mathbf{n}),$$

where minimization is constrained by the condition $\sum_{i=0}^m n_i + m = N$. This problem, in turn, is equivalent to maximizing $\phi(\mathbf{n}, m)$, which is seemingly straightforward in view of the concavity of the function $\tanh(x+1)\theta$. Thus, one can ‘naively’ conclude that the interior ‘islands’ must have the same size and that

$$n_i = \frac{N}{m} - 1. \quad (4.1)$$

For most m , however, the ratio N/m is not an integer. The actual maximum of $\phi(\mathbf{n}, m)$ is achieved on ‘almost periodic’ configurations when the components of \mathbf{n} take two values corresponding to integers nearest to $N/m - 1$ (figure 9). More precisely, the q components of the m -dimensional vector $\|n_1, \dots, n_{m-1}, n_0 + n_m\|$ must be equal to $[N/m]$, whereas the remaining $m - q$ components must be equal to $[N/m] - 1$, where $q = N - m[N/m]$. Note that the ‘naive’ analytical solution (4.1), allowing n_i to be fractional, is still useful because it provides a lower bound for the energy.

By substituting the optimal configuration \mathbf{n} into (3.6), we obtain

$$h(m) = \max_{\{\mathbf{n}, \sum_{i=0}^m n_i = N - m\}} \phi(\mathbf{n}, m) = \left\{ \frac{q}{N} \tanh \left(\left[\frac{N}{m} \right] + 1 \right) \theta + \frac{m - q}{N} \tanh \left[\frac{N}{m} \right] \theta \right\} \coth \theta.$$

This result is illustrated in figure 10a, where the actual and the ‘naive’ solutions are drawn together. The dependence of the result on E_{\perp} is illustrated in figure 10b. The ‘optimal’ metastable branches corresponding to different values of the ‘magnetization’ m are illustrated in figure 11. We see that, among configurations with the same m , the lowest energy corresponds to the ones with almost uniform distribution of cracks.

An important observation from figure 11 is that perfectly periodic configurations play a special role. To see this more clearly, it is convenient to introduce the fraction of broken springs $\omega = m/N$,

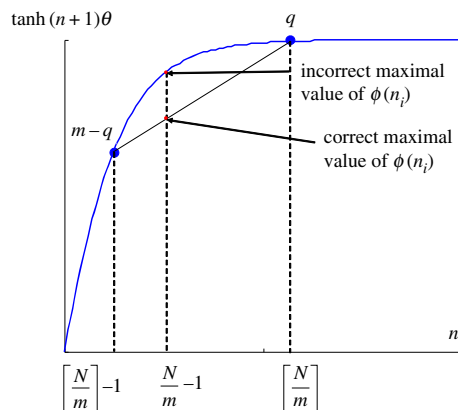


Figure 9. Geometrical illustration of the maximization of $\phi(\mathbf{n}, m)$ at a given value of m . (Online version in colour.)

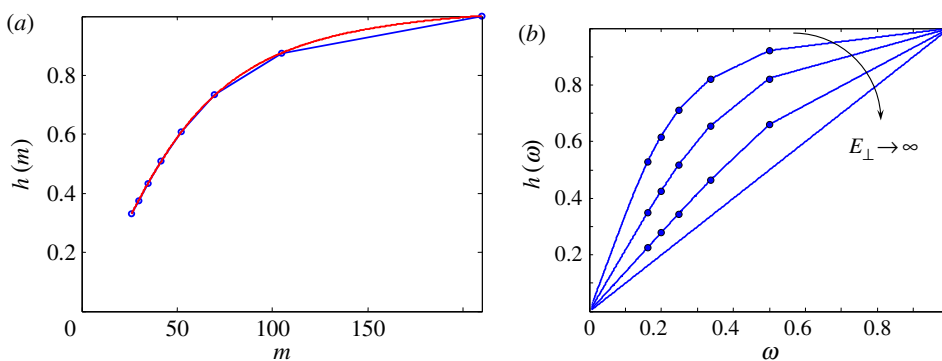


Figure 10. (a) Naive (smooth red curve) and true (blue line) maxima of $\phi(\mathbf{n}, m)$ as a function of m . Parameters: $\theta = 0.4$, $N = 210$. (b) The true function $h(\omega)$ for $\omega = m/N$ at different values of θ . (Online version in colour.)

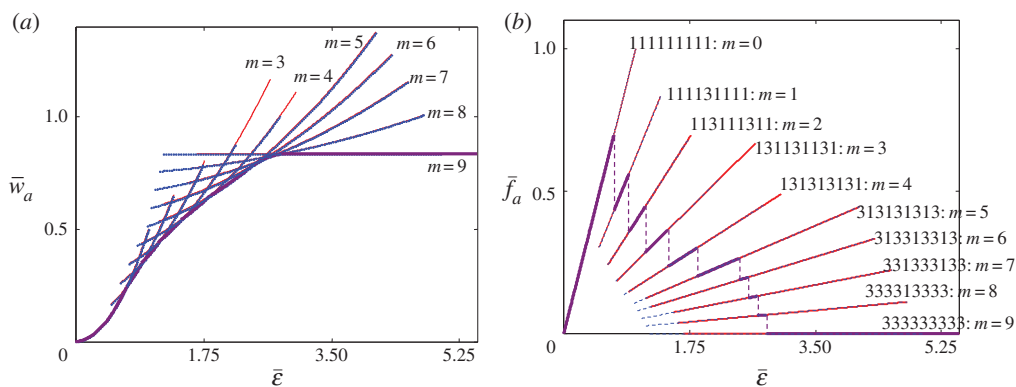


Figure 11. Optimal apparent energies and the corresponding force–strain relations for different values of parameter m in a chain with $N = 9$. Parameters: $E = 1.5$, $E_{\parallel} = 0.5$, $E_{\perp} = 1$. In contrast with figure 3 and figure 7, only the ‘optimal’ metastable branches are shown. (Online version in colour.)

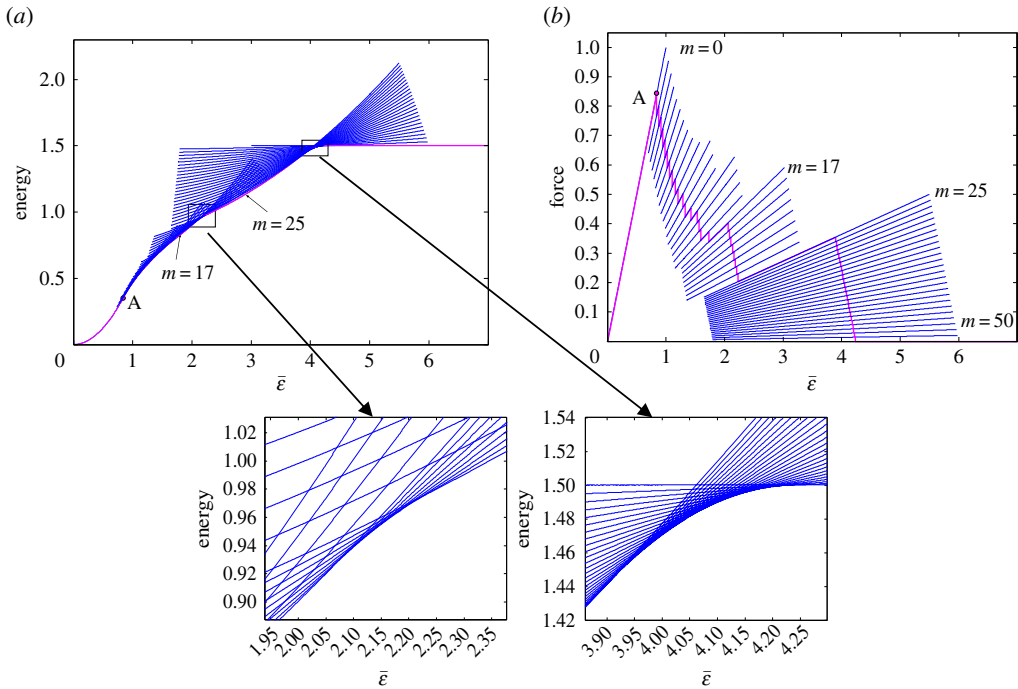


Figure 12. Apparent energy (a) and the corresponding force–strain relations (b) associated with the optimal metastable branches for the case $N = 50$. Parameters: $E = 1, E_{\parallel} = 1, E_{\perp} = 0.5$. Insets below show the blow-up of the rectangles in (a). (Online version in colour.)

and rewrite the expression for the energy at given $\bar{\varepsilon}$ and ω in the form

$$\bar{w}(\bar{\varepsilon}, \omega) = \frac{E_{\parallel}(1 + E_{\parallel})}{2(E_{\parallel} + h(\omega))} \bar{\varepsilon}^2 + \frac{\eta\omega}{2}, \quad (4.2)$$

where

$$h(\omega) = \left\{ \tanh \left(\left[\frac{1}{\omega} \right] + 1 \right) \theta - \tanh \left[\frac{1}{\omega} \right] \theta \right. \\ \left. + \omega \left(\left(1 + \left[\frac{1}{\omega} \right] \right) \tanh \left[\frac{1}{\omega} \right] \theta - \left[\frac{1}{\omega} \right] \tanh \left(\left[\frac{1}{\omega} \right] + 1 \right) \theta \right) \right\} / \tanh \theta. \quad (4.3)$$

As we see from figure 9b, the function $h(\omega)$ is continuous and piecewise linear in the interval $\omega \in (0, 1]$ with continuous first derivative everywhere except when $1/\omega$ is an integer. At such special points, the ‘optimal’ configurations are perfectly periodic, but the right and the left derivatives of $h(\omega)$ do not coincide. In the limit $E_{\perp} \rightarrow \infty$, when the long-range interactions disappear, we have $\tanh \theta \rightarrow 1$ and $h(\omega) \rightarrow \omega$, so the singular points disappear.

The last step towards global minimization of the energy is to find

$$\bar{w}(\bar{\varepsilon}) = \min_{\omega=0, 1/N, \dots, 1} \bar{w}(\bar{\varepsilon}, \omega).$$

To compute $\bar{w}(\bar{\varepsilon})$, we must identify for each ω the points of intersection of the parabolas $\bar{w}(\bar{\varepsilon}, \omega)$ with the neighbouring parabolas $\bar{w}(\bar{\varepsilon}, \omega - 1/N)$ and $\bar{w}(\bar{\varepsilon}, \omega + 1/N)$ and then check whether the function $\bar{w}(\bar{\varepsilon}, \omega)$ delivers the lowest value for the energy in the obtained interval. For a finite N , the expressions for the ‘switching’ strains can be obtained explicitly (expressions not presented here), and the result is illustrated in figure 12.

5. The continuum limit

As parameter N increases, the exact formulae describing the structure of the energy minimum $\bar{w}(\bar{\varepsilon})$ become quickly unmanageable. Analytically transparent expressions, however, can still be obtained in the continuum limit $N \rightarrow \infty$. To this end, we define the energy

$$\bar{w}(\bar{\varepsilon}, \omega) = \min_{N \rightarrow \infty} \bar{w}(\bar{\varepsilon}, m).$$

This energy would have to be minimized in the interval $\omega \in (0, 1]$. To find the optimal configuration $\omega_{\bar{\varepsilon}}$, satisfying

$$\bar{w}(\bar{\varepsilon}, \omega_{\bar{\varepsilon}}) = \inf_{\omega \in (0, 1]} \bar{w}(\bar{\varepsilon}, \omega),$$

we first note that, at regular points where $h(\omega)$ is differentiable,

$$\frac{\partial^2 \bar{w}}{\partial \omega^2} = \frac{\bar{\varepsilon}^2 (1 + E_{\parallel}) E_{\parallel} (h'(\omega))^2}{(E_{\parallel} + h(\omega))^3} > 0,$$

and therefore $\bar{w}(\bar{\varepsilon}, \omega)$ is a convex function of ω . At singular points

$$\left[\frac{\partial \bar{w}}{\partial \omega} \right]_{\omega=1/n} = \frac{\bar{\varepsilon}^2 n E_{\parallel} (1 + E_{\parallel}) (2 \tanh n\theta - \tanh(n+1)\theta - \tanh(n-1)\theta)}{2 \tanh \theta (E_{\parallel} + h(1/n))^2} > 0,$$

and here again $\bar{w}(\bar{\varepsilon}, \omega)$ is a convex function of ω .

At any given value of $\bar{\varepsilon}$, we now have two possibilities:

(a) The minimum of $\bar{w}(\bar{\varepsilon}, \omega)$ is attained at the point of differentiability, i.e. there exists $\omega \neq 1/n$ such that

$$\left. \frac{\partial \bar{w}(\bar{\varepsilon}, \omega)}{\partial \omega} \right|_{\omega=\omega_{\bar{\varepsilon}}} = 0.$$

Then

$$\omega_{\bar{\varepsilon}} = \sqrt{\frac{E_{\parallel} (1 + E_{\parallel}) \tanh \theta}{\eta ((n+1) \tanh n\theta - n \tanh(n+1)\theta)}} \bar{\varepsilon} - \frac{E_{\parallel} \tanh \theta + \tanh(n+1)\theta - \tanh n\theta}{(n+1) \tanh n\theta - n \tanh(n+1)\theta}. \quad (5.1)$$

(b) Function $\bar{w}(\bar{\varepsilon}, \omega)$ attains its the lowest value at a point ω where the derivatives experience a jump. Then, there exists

$$\omega = \frac{1}{n}, \quad n = 1, 2, \dots,$$

such that

$$\left. \frac{\partial \bar{w}(\bar{\varepsilon}, \omega)}{\partial \omega} \right|_{\omega=1/n-0} \leq 0 \quad \text{and} \quad \left. \frac{\partial \bar{w}(\bar{\varepsilon}, \omega)}{\partial \omega} \right|_{\omega=1/n+0} \geq 0.$$

This implies that, for $\bar{\varepsilon} \in (\bar{\varepsilon}_{1/n-0}, \bar{\varepsilon}_{1/n+0})$, we have

$$\bar{\varepsilon}_{1/n-0} = \left(1 + \frac{\tanh n\theta}{E_{\parallel} n \tanh \theta} \right) \sqrt{\frac{\eta E_{\parallel} \tanh \theta}{(1 + E_{\parallel}) ((n+1) \tanh n\theta - n \tanh(n+1)\theta)}} \quad (5.2)$$

$$\text{and} \quad \bar{\varepsilon}_{1/n+0} = \left(1 + \frac{\tanh n\theta}{E_{\parallel} n \tanh \theta} \right) \sqrt{\frac{\eta E_{\parallel} \tanh \theta}{(1 + E_{\parallel}) (n \tanh(n-1)\theta - (n-1) \tanh n\theta)}}.$$

The optimal configuration is then, of course,

$$\omega_{\bar{\varepsilon}} = \frac{1}{n}. \quad (5.3)$$

In figure 13a, we illustrate the ‘staircase’ $\omega(\bar{\varepsilon})$ defined by equations (5.1)–(5.3). In the interval $(\bar{\varepsilon}_0; \bar{\varepsilon}_1)$, where

$$\bar{\varepsilon}_0 = \lim_{\omega \rightarrow 0^+} \bar{\varepsilon}_{\omega} = \sqrt{\frac{\eta E_{\parallel} \tanh \theta}{1 + E_{\parallel}}} \quad \text{and} \quad \bar{\varepsilon}_1 = \lim_{\omega \rightarrow 1^-} \bar{\varepsilon}_{\omega} = \sqrt{\frac{\eta (1 + E_{\parallel}) \tanh \theta}{E_{\parallel} (2 \tanh \theta - \tanh 2\theta)}}$$

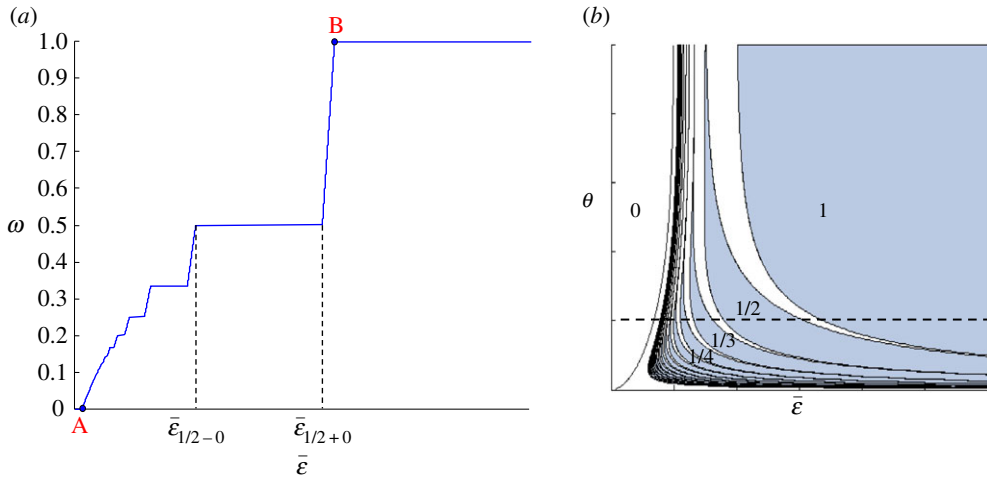


Figure 13. (a) The fraction of the phase III springs in the ground states, $\omega = m/N$, as a function of the average strain $\bar{\epsilon}$. Parameters $E_{\parallel} = 0.2$, $\theta = 0.25$, $\eta = 2$. (b) The θ - $\bar{\epsilon}$ phase diagram: shaded areas correspond to purely periodic phases; the number inside each shaded area reflects the fraction of springs in phase III. (Online version in colour.)

(points A and B in figure 13a), the deformation is inhomogeneous and elements in both phases I and III are present. Outside this interval, the deformation is homogeneous, with all springs either broken or unbroken and with ω equal either 0 or 1. Observe the accumulation of the steps on the AB segment around point A; this feature allows us to qualify this curve as an incomplete devil's staircase.

In figure 13b, we show the θ versus $\bar{\epsilon}$ phase diagram for $E_{\parallel} = 1$. On this diagram, we indicate the domains of global stability of various purely periodic configurations (5.3). The boundaries between these domains are defined by (5.2). We see once again that when $\theta \rightarrow \infty$, which at a fixed E_{\parallel} means that $E_{\perp} \rightarrow \infty$, the periodic patterns do not survive as singular states and become indistinguishable from other configurations.

The lower envelope of the family of curves $\bar{w}(\bar{\epsilon}, \omega)$ is given explicitly by the expressions:

$$\bar{w}(\bar{\epsilon}) = \begin{cases} \sqrt{\frac{E_{\parallel}(1+E_{\parallel})\eta \tanh \theta}{(n+1) \tanh n\theta - n \tanh(n+1)\theta} \bar{\epsilon} - \frac{\eta(E_{\parallel} \tanh \theta + (\tanh(n+1)\theta - \tanh n\theta))}{2((n+1) \tanh n\theta - n \tanh(n+1)\theta)}}, & \bar{\epsilon} \in \left(\bar{\epsilon}_{\frac{1}{n+1}+0}, \bar{\epsilon}_{\frac{1}{n}-0} \right), \\ \frac{E_{\parallel}(1+E_{\parallel})}{2(E_{\parallel} + \tanh n\theta/n \tanh \theta)} \bar{\epsilon}^2 + \frac{\eta}{2n}, & \bar{\epsilon} \in \left(\bar{\epsilon}_{\frac{1}{n}-0}, \bar{\epsilon}_{\frac{1}{n}+0} \right), \\ \frac{(1+E_{\parallel})}{2} \bar{\epsilon}^2, & \bar{\epsilon} \in (0, \bar{\epsilon}(0)). \end{cases} \quad (5.4)$$

According to (5.4), the function $\bar{w}(\bar{\epsilon})$ is a convex envelope of a family of parabolas:

$$\bar{w}_n(\bar{\epsilon}) = \frac{E_{\parallel}(1+E_{\parallel})}{2(E_{\parallel} + \tanh n\theta/n \tanh \theta)} \bar{\epsilon}^2 + \frac{\eta}{2n}. \quad (5.5)$$

It contains linear segments

$$\bar{w}_{n,n+1}(\bar{\epsilon}) = \sqrt{\frac{E_{\parallel}(1+E_{\parallel})\eta \tanh \theta}{(n+1) \tanh n\theta - n \tanh(n+1)\theta} \bar{\epsilon} - \frac{\eta(E_{\parallel} \tanh \theta + (\tanh(n+1)\theta - \tanh n\theta))}{2((n+1) \tanh n\theta - n \tanh(n+1)\theta)}}, \quad (5.6)$$

corresponding to common tangent constructions linking parabolas $\bar{w}_n(\bar{\epsilon})$ and $\bar{w}_{n+1}(\bar{\epsilon})$. We note, again without presenting the explicit condition, that for the validity of this solution the single-spring force-strain relation in the spinodal region should be sufficiently steep.

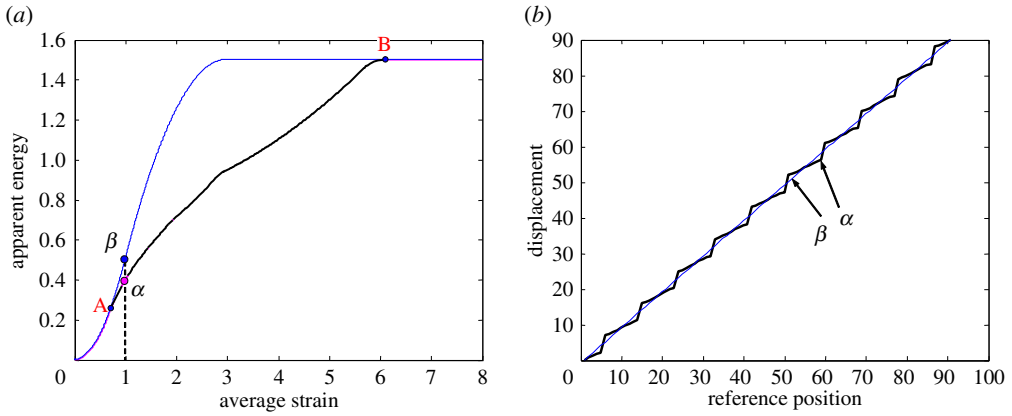


Figure 14. (a) Apparent energy along the global minimum path (bold black line), and the energy along the homogeneous deformation path (solid blue line) for the system with $N = 90$. Parameters: $E = 0.5$, $E_{\parallel} = 1$, $E_{\perp} = 0.2$. (b) The displacement field \mathbf{u} corresponding to the global minimizer of the energy (point α in (a)) compared with the displacement field for a homogeneous deformation (point β in (a)). (Online version in colour.)

The structure of the apparent energy along the global minimum path is illustrated in figure 14a. To emphasize the energetic advantage for the system to be microscopically non-uniform in the range of interest, we also plot on the same graph the apparent energy for a microscopically uniform system. Note that, although the ground state loses its microscopic homogeneity (between points A and B), the coarse-grained deformation field remains homogeneous (figure 14b).

The force, $f(\bar{\varepsilon})$, along the global minimum path can be calculated from the expression

$$\left. \frac{\partial \bar{w}(\bar{\varepsilon}, \omega)}{\partial \bar{\varepsilon}} \right|_{\omega=\omega_{\bar{\varepsilon}}} = f(\bar{\varepsilon}, \omega_{\bar{\varepsilon}}) \equiv f(\bar{\varepsilon}).$$

The result can again be written explicitly:

$$f(\bar{\varepsilon}) = \begin{cases} \sqrt{\frac{E_{\parallel}(1+E_{\parallel})\eta \tanh \theta}{(n+1) \tanh n\theta - n \tanh(n+1)\theta}} = \text{const}, & \bar{\varepsilon} \in \left(\bar{\varepsilon}_{\frac{1}{n+1}+0}, \bar{\varepsilon}_{\frac{1}{n}-0} \right), \\ \frac{E_{\parallel}(1+E_{\parallel})}{E_{\parallel} + \tanh n\theta/n \tanh \theta} \bar{\varepsilon}, & \bar{\varepsilon} \in \left(\bar{\varepsilon}_{\frac{1}{n}-0}, \bar{\varepsilon}_{\frac{1}{n}+0} \right), \\ (1+E_{\parallel})\bar{\varepsilon}, & \bar{\varepsilon} \in (0, \bar{\varepsilon}(0)). \end{cases} \quad (5.7)$$

By subtracting $E_{\parallel}\bar{\varepsilon}$ from (5.7), we can also write an explicit expression for the apparent force-strain relation:

$$f_a = f - E_{\parallel}\bar{\varepsilon} = \begin{cases} -E_{\parallel}\bar{\varepsilon} + \sqrt{\frac{E_{\parallel}(1+E_{\parallel})\eta \tanh \theta}{(n+1) \tanh n\theta - n \tanh(n+1)\theta}}, & \bar{\varepsilon} \in \left(\bar{\varepsilon}_{\frac{1}{n+1}+0}, \bar{\varepsilon}_{\frac{1}{n}-0} \right), \\ \frac{E_{\parallel}(n \tanh \theta - \tanh n\theta)}{E_{\parallel} n \tanh \theta + \tanh n\theta} \bar{\varepsilon}, & \bar{\varepsilon} \in \left(\bar{\varepsilon}_{\frac{1}{n}-0}, \bar{\varepsilon}_{\frac{1}{n}+0} \right), \\ \bar{\varepsilon}, & \bar{\varepsilon} \in (0, \bar{\varepsilon}(0)). \end{cases} \quad (5.8)$$

The asymptotic expressions obtained for $f(\bar{\varepsilon})$ and $f_a(\bar{\varepsilon})$ are illustrated in figure 15, where we juxtapose the maximally stable (global minimum) path with the minimally stable (marginal equilibrium) path. We recall that the latter can be viewed as the outcome of the quasi-static overdamped dynamics [21].

An important feature of the relaxed energy is the presence of a set of embedded linear segments responsible for the intricate system of steps on the force-elongation curve. In those states, the system is locked into ‘rational’ geometrical patterns. Such steps carry the memory

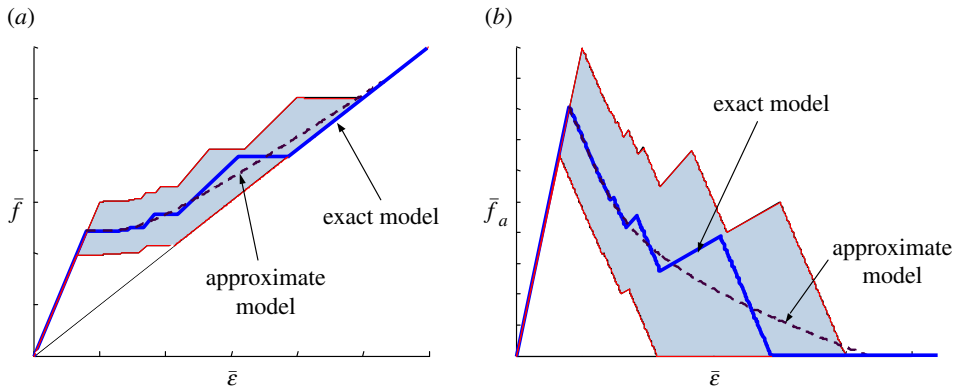


Figure 15. Actual (a) and apparent (b) force–strain relations in the continuum limit. Parameters: $E = 0.5$, $E_{\parallel} = 0.5$, $E_{\perp} = 1$. The global minimum path is shown by a thick blue line, the two-way marginally stable path is shown by the thin red line, the ‘naive’ approximation explained in the text is shown by a dashed line. (Online version in colour.)

about the inherent discreteness of the original problem and cannot be recovered from the straightforward quasi-continuum approximations (see the dashed lines in figure 15). Construction of a continuum fracture energy whose relaxation agrees with the pattern shown in figure 15 presents an interesting mathematical challenge: examples with somewhat similar behaviour can be found [22].

6. Conclusion

The goal of the study of a one-dimensional chain with cohesive/brittle elements was to reveal the complexity of the metastable patterns in the brittle–elastic systems and to elucidate the origin of the locking phenomenon. The patterning in this model can be understood in terms of the competition between incommensurate interactions. The non-convexity of the elastic energy of brittle springs drives the system towards strain localization, while the elastic background with convex energy favours homogeneity. In the absence of an internal length scale, this competition leads to the formation of an infinite number of infinitesimal cracks. The discreteness of the problem supplies the length scale responsible for the finite scale of the microstructures.

The striking structural stability of the commensurate microstructures in this model is manifested by the fact that, even in the continuum limit, the infinitesimal parameter variation does not affect their robust topological structure. Such locking was observed in experiments on self-assembly of micropillars in drying systems [4] but has not been previously rationalized at the conceptual level [14]. Robustness of this type can play an important role in stress-induced developmental morphogenesis, ensuring, for instance, that the number of fingers or vertebra is largely independent of the variation of external parameters [9].

The insights provided by the study of this conceptual model have to be corroborated by two- and three-dimensional models aimed at reproducing realistic geometries and capturing the specificity of elastic and cohesive interactions. Furthermore, our static analysis should be supplemented by the study of dynamics, allowing one to distinguish between different paths in the rugged energy landscapes characterizing this type of systems. Finally, it will be important to show the limited sensitivity of the predicted locking patterns to the randomness of the breaking thresholds [11].

Authors’ contributions. Both authors participated in the mathematical analysis and the writing of the manuscript. Both authors gave final approval for publication.

Competing interests. We declare we have no competing interests.

Funding. This work was supported by the NSF under grant no. DMS-0102841.

Acknowledgements. The authors thank J. Aizenberg and U. Salman for helpful discussions. This work is part of the PhD thesis defended by I.N. in 2002 at the University of Minnesota. L.T. thanks NSF grant DMS-0102841 for supporting this project.

References

- Hutchinson J, Suo Z. 1991 Mixed mode cracking in layered materials. *Adv. Appl. Mech.* **29**, 63–191. (doi:10.1016/S0065-2156(08)70164-9)
- Bourdin B, Francfort G, Marigo J-J. 2008 The variational approach to fracture. *J. Elast.* **91**, 5–148. (doi:10.1007/s10659-007-9107-3)
- Vellinga WP, Van den Bosch M, Geers MGD. 2008 Interaction between cracking, delamination and buckling in brittle elastic thin films. *Int. J. Fract.* **154**, 195–209. (doi:10.1007/s10704-008-9266-7)
- Pokroy B, Kang SH, Mahadevan L, Aizenberg J. 2009 Self-organization of a mesoscale bristle into ordered, hierarchical helical assemblies. *Science* **323**, 237–240. (doi:10.1126/science.1165607)
- Geim A, Dubonos SV, Grigorieva IV, Novoselov KS, Zhukov AA, Shapoval SY. 2003 Microfabricated adhesive mimicking gecko foot-hair. *Nat. Mater.* **2**, 461–463. (doi:10.1038/nmat917)
- Chakrapani N, Wei B, Carrillo A, Ajayan PM, Kane RS. 2004 Capillarity-driven assembly of two-dimensional cellular carbon nanotube foams. *Proc. Natl Acad. Sci. USA* **101**, 4009–4012. (doi:10.1073/pnas.0400734101)
- Corson F, Henry H, Adda-Bedia M. 2010 A model for hierarchical patterns under mechanical stresses. *Philos. Mag.* **90**, 357–373. (doi:10.1080/14786430903196665)
- Mirabet V, Das P, Boudaoud A, Hamant O. 2011 The role of mechanical forces in plant morphogenesis. *Annu. Rev. Plant Biol.* **62**, 365–385. (doi:10.1146/annurev-arplant-042110-103852)
- Truskinovsky L, Vitale G, Smit TH. 2014 A mechanical perspective on vertebral segmentation. *Int. J. Eng. Sci.* **83**, 124–137. (doi:10.1016/j.jengsci.2014.05.003)
- Novak I, Truskinovsky L. 2014 Nonaffine response of skeletal muscles on the ‘descending limb’. *Math. Mech. Solids* **20**, 697–720. (doi:10.1177/1081286514551504)
- Morgenstern I, Sokolov IM, Blumen A. 1993 Analysis of a one-dimensional fracture model. *J. Phys. A: Math. Gen.* **26**, 4521. (doi:10.1088/0305-4470/26/18/019)
- Hornig T, Sokolov IM, Blumen A. 1996 Patterns and scaling in surface fragmentation processes. *Phys. Rev. E* **54**, 4293. (doi:10.1103/PhysRevE.54.4293)
- Handge UA, Leterrier Y, Rochat G, Sokolov IM, Blumen A. 2000 Two scaling domains in multiple cracking phenomena. *Phys. Rev. E* **62**, 7807. (doi:10.1103/PhysRevE.62.7807)
- Wei Z, Schneider TM, Kim J, Kim H-Y, Aizenberg J, Mahadevan L. 2015 Elastocapillary coalescence of plates and pillars. *Proc. R. Soc. A* **471**, 20140593. (doi:10.1098/rspa.2014.0593)
- Meakin P. 1987 A simple model for elastic fracture in thin films. *Thin Solid Films* **151**, 165–190. (doi:10.1016/0040-6090(87)90231-8)
- Charmet JC, Guyon E, Roux S (eds). 1990 *Disorder and fracture*, NATO ASI Series B, vol. 204. New York, NY: Plenum Press. (doi:10.1007/978-1-4615-6864-3)
- Truskinovsky L. 1996 Fracture as a phase transition. In *Contemporary research in the mechanics and mathematics of materials* (eds R Batra, M Beatty), pp. 322–332. Barcelona, Spain: International Center for Numerical Methods in Engineering (CIMNE).
- Puglisi G, Truskinovsky L. 2000 Mechanics of a discrete chain with bi-stable elements. *J. Mech. Phys. Solids* **48**, 1–27. (doi:10.1016/S0022-5096(99)00006-X)
- Griffiths RB. 1990 Frenkel–Kontorova models of commensurate–incommensurate phase transitions. In *Fundamental problems in statistical mechanics VII: Proc. 7th Int. Summer School on Fundamental Problems in Statistical Mechanics, Altenburg, FR Germany, 18–30 June 1989* (ed. H van Beijeren), pp. 69–110. Amsterdam, The Netherlands: North-Holland.
- Truskinovsky L, Vainchtein A. 2004 The origin of nucleation peak in transformational plasticity. *J. Mech. Phys. Solids* **52**, 1421–1446. (doi:10.1016/j.jmps.2003.09.034)
- Puglisi G, Truskinovsky L. 2005 Thermodynamics of rate-independent plasticity. *J. Mech. Phys. Solids* **53**, 655–679. (doi:10.1016/j.jmps.2004.08.004)
- Braides A, Truskinovsky L. 2008 Asymptotic expansions by Γ -convergence. *Contin. Mech. Thermodyn.* **20**, 21–62. (doi:10.1007/s00161-008-0072-2)